ASME Journal of Biomechanical Engineering
Online journal at:
https://asmedigitalcollection.asme.org/biomechanical

Sofia Altieri Correa
Department of Biomedical Engineering,
University of California, Irvine,
Irvine, CA 92617;
Edwards Lifesciences Foundation Cardiovascular
Innovation and Research Center,
University of California, Irvine,
Irvine, CA 92617
e-mail: altieris@uci.edu

Amirreza Kachabi
Department of Biomedical Engineering,
University of California, Irvine,
Irvine, CA 92617;
Edwards Lifesciences Foundation Cardiovascular
Innovation and Research Center,
University of California, Irvine,
Irvine, CA 92617
e-mail: akachabi@uci.edu

Mitchel J. Colebank
Department of Biomedical Engineering,
University of California, Irvine,
Irvine, CA 92617;
Edwards Lifesciences Foundation Cardiovascular
Innovation and Research Center,
University of California, Irvine,
Irvine, CA 92617;
Department of Mathematics,
University of South Carolina,
Columbia, SC 29225
e-mail: mjcolebank@sc.edu

Christopher E. Miles
Center for Complex Biological Systems,
University of California, Irvine,
Irvine, CA 92617;
Department of Mathematics,
University of California, Irvine,
Irvine, CA 92617
e-mail: cemiles@uci.edu

Naomi C. Chesler
Department of Biomedical Engineering,
University of California, Irvine,
Irvine, CA 92617;
Edwards Lifesciences Foundation Cardiovascular
Innovation and Research Center,
University of California, Irvine,
Irvine, CA 92617
e-mail: nchesler@uci.edu

Revisiting Murray's Law in Pulmonary Arteries: Exploring Branching Patterns and Principles

In 1926, Cecil D. Murray published a fundamental law of physiology relating the form and function of branched vessels. Murray's Law predicts that the diameter of a parent vessel branching into two child branches is mathematically related by a cube law based on parabolic flow and power minimization with vascular volume. This law is foundational for computational analyses of branching vascular structures. However, pulmonary arteries exhibit morphometric and hemodynamic characteristics that may deviate from classical predictions. This study investigates the morphometry of pulmonary arterial networks, examining relationships between parent and child vessel diameters across species. We analyzed three-dimensional segmentations of pulmonary arterial geometries from healthy subjects across four species: human ($n=7$), canine ($n=5$), swine ($n=4$), and murine ($n=3$). Our findings reveal an average exponent value of 2.31($\pm$0.60) in human, 2.13 ($\pm$0.54) in canine, 2.10($\pm$0.49) in swine, and 2.59($\pm$0.58) in murine, all lower than the predicted value of 3.0 from Murray's Law. Extending Murray's Law to fully developed pulsatile flow based on minimal impedance, we show that mean flow is proportional to radius raised to a power between 2.1 and 3, depending on the Womersley number. Our findings suggest that while Murray's Law provides a useful baseline, pulmonary artery (PA) branching follows a different optimization principle depending on Womersley number. This study contributes to a deeper understanding of pulmonary arterial structure–function relationships and implications for vascular disease modeling. [DOI: 10.1115/1.4068886]

Keywords: Murray's Law, vascular network morphometry, pulmonary arterial networks, branching patterns, energetic cost function, pulsatile flow, Womersley number

Introduction

The morphometry of vascular networks has been the topic of numerous studies for over 100 years [1–14]. In 1926, Cecil D. Murray formulated the most well-recognized structure–function

Manuscript received September 12, 2024; final manuscript received June 3, 2025; published online June 20, 2025. Assoc. Editor: Craig Goergen.

relation for the optimal branching pattern of vascular networks based on a minimum power principle [1]. He introduced a cost function that balanced the pressure-flow power required to pump blood with the metabolic power required to maintain blood temperature. Assuming steady, fully developed laminar flow of a Newtonian fluid in all vessels, and that metabolic power is proportional to blood volume, Murray predicted that volumetric blood flow rate in any branching vessel (parent or child) is proportional to the cube of its diameter. A corollary prediction is that the parent diameter cubed is equal to the sum of the child branch diameters cubed, i.e.,

$$r_0^3 = r_1^3 + r_2^3 \tag{1}$$

where r_0 represents the radius of the parent vessel, and r_1 and r_2 denote the radii of the child vessels of the bifurcation. This relationship is known as Murray's Law or the Cube Law.

Since 1926, variations of Murray's approach have been developed, first by Uylings [3] who considered steady fully developed turbulent flow, and then by Stephenson and Lockerby [7] who considered steady fully developed laminar and turbulent flow in noncylindrical vessel shapes and fully developed laminar flow of non-Newtonian fluids in cylindrical vessel shapes. Despite the well-known unsteadiness of physiological flow phenomena (including both blood in the circulation and air in the lung) and an analytical solution to fully developed pulsatile flow of a Newtonian fluid in a cylindrical vessel (Womersley), the impact of the steady flow assumption on Murray's Law was not considered until much later by West et al. [8] and then Painter et al. [9], who only achieved qualitative results. Very recently, a quantitative solution was developed [10] but missing information in the derivation prevent wide acceptance and adoption. Here, we provide a new analysis of Murray's minimum power principles using impedance to derive the quantitative dependence of exponent on Womersley number for nonzero-mean pulsatile flow.

To investigate the applicability of the traditional (steady) and modified (unsteady) Murray's Law to the pulmonary circulation, we examined the relationships between parent and child diameters in pulmonary arterial networks across four different species, using healthy subjects only. We analyze three-dimensional (3D) reconstructions of pulmonary arterial trees by reducing their geometries to a quantifiable network graph, including vessel connectivity, radii, and lengths. After quantifying these parameters, we assess how the Murray exponent varies with species and as a function of the Womersley number. By doing so, we seek to validate the applicability of Murray's Law to pulmonary arteries and to explore potential alternative principles governing their branching patterns. Our reanalysis of the pulmonary circuit, using new hemodynamically consistent assumptions, offers fresh insights into the structure–function relationship within the pulmonary arterial tree.

Methods

Power Minimization Analysis. Murray was the first to establish a link between the radius and flow rate of a vessel segment. He introduced an energetic cost function, denoted as P_{total}, which sums the power required to pump blood (flow, Q (ml/s), multiplied by pressure drop, ΔP (Pa)) with the metabolic cost to maintain body temperature for a single vessel of radius r and length L (assumed to be proportional to blood volume, $\pi r^2 L$, Eq. (2)), where K_1 is an unknown constant with units of (kg m^{-1} s^{-3})

$$P_{\text{total}} = Q\Delta P + K_1\,\pi\, r^2 L \tag{2}$$

Assuming fully developed laminar flow within a rigid vessel and a Newtonian fluid viscosity μ, the power for blood pumping can be approximated using Poiseuille flow (Eq. (3))

$$P_{\text{total}} = \frac{8\mu L}{\pi r^4} Q^2 + K_1\,\pi\, r^2 L \tag{3}$$

In accordance with Murray's minimum principle, when Eq. (3) is differentiated with respect to radius and minimized (i.e., set to zero), an optimal condition exists (Eq. (4)) and for these assumptions flow rate Q is proportional to the cube of radius (Eq. (5))

$$Q^2 = \left(\frac{K_1 \pi^2}{16\mu}\right) r^6 \tag{4}$$

$$\Rightarrow Q \propto r^3 \tag{5}$$

Because flow is conserved at any branching, $Q_0 = Q_1 + Q_2$, where Q_0 is the flow in the parent vessel and Q_1, Q_2 are the flows in the child vessels, hence

$$r_0^3 = r_1^3 + r_2^3 \tag{6}$$

However, if the flow becomes pulsatile with nonzero mean (Eq. (7)), the mean power, H, over a cardiac cycle with frequency ω is computed as the integral of the pressure times the flow over a single cycle (Eq. (8)) which results in a solution in terms of A, B that is challenging to relate to r

$$Q(t) = A + Be^{i\omega t} \tag{7}$$

$$H = \int_{-\pi/\omega}^{\pi/\omega} \Delta P(t) Q(t) \mathrm{d}t \tag{8}$$

Impedance Analysis for Steady Flow. Instead of the above analysis, an argument that dates to Sherman [11] and has been used several times since, e.g., Refs. [10,12], and [13], states that pulmonary vascular impedance can be minimized subject to throughput constraints again assuming fully developed laminar flow within a rigid vessel and a Newtonian fluid viscosity μ.

First, to show this line of reasoning recapitulates Murray's Law, we consider a parent vessel with radius r_0 that splits into two child branches of equal radii r_1. The total volume in this junction is

$$V_{\text{tot}} = \pi r_0^2 \ell_0 + (2)\pi r_1^2 \ell_1 \tag{9}$$

Hagen–Poiseuille's Law says the impedance (resistance) through a branch with r and length ℓ is

$$Z = \frac{\Delta P}{Q} = \frac{8\mu\ell}{\pi r^4} \tag{10}$$

As the two child vessels are parallel and in series with the parent, the total impedance is

$$Z_{\text{tot}} = Z_0 + \frac{Z_1}{2} = \frac{8\mu\ell_0}{\pi r_0^4} + \frac{8\mu\ell_1}{2\pi r_1^4} \tag{11}$$

Next, consider a cost function where the impedance is minimized subject to the constraint that $V = V_{\text{tot}}$ implemented by a Lagrange multiplier

$$C = Z_{\text{tot}} + \lambda(V_{\text{tot}} - V) = \frac{8\mu\ell_0}{\pi r_0^4} + \frac{8\mu\ell_1}{2\pi r_1^4} + \lambda\left[\pi r_0^2 \ell_0 + 2\pi r_1^2 \ell_1 - V\right] \tag{12}$$

We can now take derivatives of this cost function with respect to each radius

$$\partial_{r_0} C = 0 \Longrightarrow \lambda = \frac{16\mu}{\pi^2 r_0^6}, \quad \partial_{r_1} C = 0 \Longrightarrow \lambda = \frac{4\mu}{\pi^2 r_1^6} \tag{13}$$

Since the child vessel will be smaller than the parent vessel, we can set $r_1 = \beta r_0$, where $\beta < 1$. Then, setting the two derivatives of the cost function equal to each other provides the optimal relation between r_0 and β

$$\frac{4\left(-1+4\beta^6\right)\mu}{\pi^2 r_0 \beta^6}=0 \text{ or } -1+4\beta^6=0 \text{ or } \left(2\beta^3-1\right)\left(2\beta^3+1\right)=0 \tag{14}$$

such that $\beta = 2^{-1/3}$ is recovered, since β cannot be less than zero, which is exactly Murray's Law

$$\begin{aligned} 0 &= r_1^3 + r_1^3 - r_0^3 = (\beta r_0)^3 + (\beta r_0)^3 - r_0^3 \\ &= r_0^3\left(2\beta^3-1\right) \text{ or } \left(2\beta^3-1\right)=0 \end{aligned} \tag{15}$$

Impedance Analysis for Nonzero-Mean Pulsatile Flow. The general calculation for nonzero mean pulsatile flow is nearly identical to the previous one for steady flow, except that the impedance is now a complex, frequency domain quantity. The volume constraint remains the same, and we still assume two child branches of equal radii. The total impedance becomes the sum of the steady and oscillatory components

$$\begin{aligned} Z_{\text{tot}} = Z_0 + \frac{Z_1}{2} &= \frac{8\mu\ell_0}{\pi r_0^4} + \frac{8\mu\ell_1}{2\pi r_1^4} + \frac{\omega\rho}{i\pi} \\ &\times \left(\frac{\ell_0 J_0\left(i^{3/2}\sqrt{\frac{\omega\rho}{\mu}}r_0\right)}{r_0^2 J_2\left(i^{3/2}\sqrt{\frac{\omega\rho}{\mu}}r_0\right)} + \frac{\ell_1 J_0\left(i^{3/2}\sqrt{\frac{\omega\rho}{\mu}}r_1\right)}{2r_1^2 J_2\left(i^{3/2}\sqrt{\frac{\omega\rho}{\mu}}r_1\right)} \right) \end{aligned} \tag{16}$$

The second terms are textbook expressions (see, for instance, Ref. [14]) for the impedance of oscillatory flow $Z = \Delta P/Q$, where $i = \sqrt{-1}$ and ρ is the blood density. For now, we abbreviate $\kappa := \sqrt{\omega\rho/\mu}$.

Again, we consider the cost function

$$C = Z_{\text{tot}} + \lambda(V_{\text{tot}} - V) \tag{17}$$

The derivatives here are straightforward to compute in terms of Bessel functions defined by $I_\alpha(x) := i^{-\alpha}J_\alpha(ix)$

$$\partial_{r_0} C = 4\ell_0\pi r_0\lambda - \frac{32\ell_0\mu}{\pi r_0^5} - \frac{2i\ell_0\rho\omega I_1\left(i^{1/4}\kappa r_0\right)^2}{\pi r_0^3 I_2\left(i^{1/4}\kappa r_0\right)^2} \tag{18}$$

and

$$\partial_{r_1} C = 8\ell_1\pi r_1\lambda - \frac{16\ell_1\mu}{\pi r_1^5} - \frac{i\ell_1\rho\omega I_1\left(i^{\frac{1}{4}}\kappa r_1\right)^2}{\pi r_1^3 I_2\left(i^{\frac{1}{4}}\kappa r_1\right)^2} \tag{19}$$

Solving each for λ provides the two conditions

$$\lambda = \frac{8\mu}{\pi^2 r_0^6} + \frac{i\rho\omega}{2\pi^2 r_0^4}\frac{I_1\left(i^{1/4}\kappa r_0\right)^2}{I_2\left(i^{1/4}\kappa r_0\right)^2} = \frac{2\mu}{\pi^2 r_1^6} + \frac{i\rho\omega}{8\pi^2 r_1^4}\frac{I_1\left(i^{1/4}\kappa r_1\right)^2}{I_2\left(i^{1/4}\kappa r_1\right)^2} \tag{20}$$

If we again replace $r_1 = \beta r_0$, we can set these expressions equal and find an expression for β

$$\begin{aligned} 0 = g(\beta) &= 16\mu\left(4-\beta^{-6}\right) \\ &+ ir_0^2\rho\omega\left(\frac{4I_1\left(i^{1/4}\kappa r_0\right)^2}{I_2\left(i^{1/4}\kappa r_0\right)^2} - \frac{I_1\left(i^{1/4}\kappa\beta r_0\right)^2}{\beta^4 I_2\left(i^{1/4}\kappa\beta r_0\right)^2}\right) \end{aligned} \tag{21}$$

Importantly, $g(\beta)$ is complex valued, so we must interpret this as $0 = |g(\beta)|$, the modulus.

Moreover, we can identify the Womersley number (Wo) of the inlet

$$\text{Wo} = r_0\kappa = r_0\sqrt{\frac{\rho\omega}{\mu}} \tag{22}$$

and our expression reduces to

$$0 = g(\beta) = \mu\left(64 - \frac{16}{\beta^6} + \frac{4iI_1\left(i^{1/4}\text{Wo}\right)^2}{I_2\left(i^{1/4}\text{Wo}\right)^2} - \frac{iI_1\left(i^{1/4}\beta\text{Wo}\right)^2}{\beta^4 I_2\left(i^{1/4}\beta\text{Wo}\right)^2}\right) \tag{23}$$

Importantly, this shows that the expression is *solely* dependent on the Womersley number (Wo). We can numerically determine the value of β that satisfies Eq. (23) for any given Wo value, thereby generating the relationship between Murray's exponent and Womersley number where the Murray's exponent is set as $x(\text{Wo}) = 1/\log_2\left(1/\beta(\text{Wo})\right)$. The quantitative result is consistent with the previous qualitative results of Refs. [8] and [9] but not identical to the solution obtained by Shumal et al. [10].

Pulmonary Arterial Tree Image Analysis. Computed tomography or magnetic resonance angiography (MRa) images of the pulmonary arterial tree from seven healthy adult humans (four males and three females, aged 15 to 51) were obtained from the Vascular Model Repository [15]. For swine, MRa images from four young female pigs (56±24 kg body weight) obtained as part of a separate study [16] were used. For canines, MRa images from five healthy adult male beagles (12±1 kg body weight) obtained as part of a separate study [17] were used. Finally, murine data were derived from three microcomputed tomography images of three healthy excised male C57BL6/J mouse lungs (10- to 12-weeks-old) with contrast-perfused pulmonary arteries [18]. An average of 6±1 generations of the pulmonary arterial tree were analyzed in each of the four species.

The workflow is outlined in Fig. 1. First, we created 3D segmentations of pulmonary artery (PA) geometries using 3D SLICER

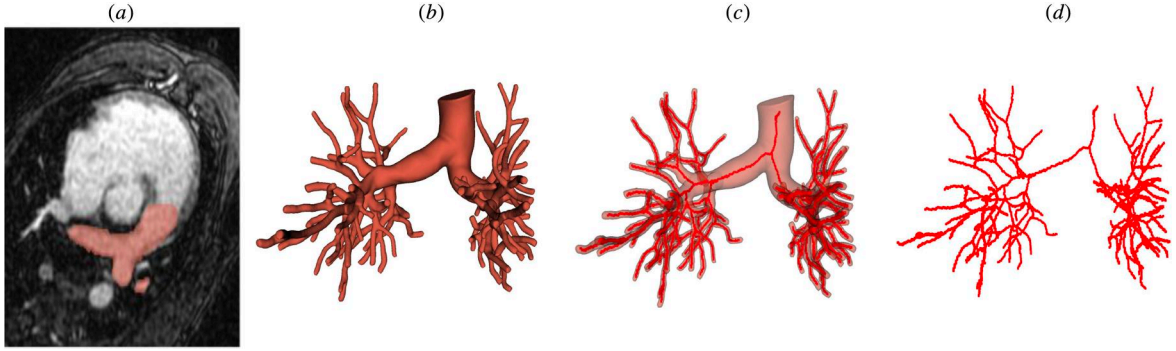

Fig. 1 Pulmonary artery branching pattern analysis workflow, including (*a*) arterial identification from images, (*b*) 3D segmentations of the arterial network, and (*c*) and (*d*) network extraction from the 3D segmentations

[19]. Then, the network was extracted using SpatialGraph Extractor (SGEXT) [20]. We generated a thin/skeletonized image from binary segmentations, maintaining the topology of the input binary image. Using a distance map ensures that the thin image is centered along the PA centerline. The resulting thin output is then converted into a spatial graph, which consists of an adjacency list storing nodes and edges along with their corresponding geometric information. Nodes are represented as spatial points with 3D locations, while edges are defined as spatial structures containing a sequence of points that connect the nodes. Finally, we postprocessed the extracted networks using custom MATLAB software, obtaining length, radius, and connectivity data for each network [21].

Womersley Number Estimation. The Womersley number (Wo) is a dimensionless parameter that characterizes the unsteadiness of pulsatile flow in relation to viscous effects. We estimated Wo for each species at the main pulmonary artery (MPA), a consistently identifiable vessel across species. Assuming a blood density (ρ) of 1.050 g/cm^3 and a Newtonian viscosity (μ) of 4.0 cP, we used the MPA radius from imaging data along with measured heart rates (HRs) for each subject in canines and swine to calculate Wo. Since we did not have measured heart rate data for humans and murine, we assumed an appropriate range for them using Refs. [22] and [23], respectively.

Exponent Calculation. Following the extraction of radius values for all branches in human, swine, canine, and murine datasets, we computed the exponent (x) in Eq. (24) for each bifurcation in each subject. This calculation was performed by minimizing the difference between Eq. (24) and the measured data using MATLAB's fzero function

$$r_0^x = r_1^x + r_2^x \tag{24}$$

To evaluate whether the exponents predicted by the Womersley-based optimization deviate from the classical Murray's Law prediction (3.0), we performed a one-sample t-test on theoretical values restricted to the physiological range of 2.1 to 3.0, using MATLAB software. Additionally, one-sample t-tests were conducted on experimental data to evaluate deviations from Murray's Law across species.

Results

Table 1 presents the mean exponent values across different species, each of which were lower than the predicted value of 3.0 from the traditional Murray's Law. While the experimental values were not different from the traditional Murray's Law in humans, they were for swine, canine, and human. Averaging across all bifurcations in all species, the mean exponent was 2.43±0.32 (mean±SD), which was significantly lower than the theoretical Murray value ($p < 0.0001$).

We estimated Womersley number (Wo) for each species at the MPA, with geometric and hemodynamic assumptions and results shown in Table 2.

Figure 2 depicts the theoretical relationship between Murray's exponent and Womersley number, derived from Eq. (23) for $0 < \mathrm{Wo} < 25$, along with species-specific MPA Womersley numbers and their corresponding Murray exponents derived from imaging data. The theoretical curves align well with canine, swine, and some human data, but deviate from murine data.

Table 1 Exponent values for pulmonary artery branching patterns in human, swine, canine, and murine subjects and *p*-values for one-sample *t*-tests to evaluate deviations from Murray's prediction of 3.0

Species	Exponent (mean±SD)	p-value
Human	2.31±0.60	0.3721
Swine	2.10±0.49	**0.0166**
Canine	2.13±0.54	**0.0011**
Murine	2.59±0.58	**0.0309**

Significant difference ($p < 0.05$) indicated by bold.

Table 2 MPA radius, HR, and Womersley numbers (Wo) for all different species at MPA

Species	MPA radius (cm)	HR (bpm)	$\mathrm{Wo}_{\mathrm{MPA}}$
Human	1.00 ± 0.13	60–90	11.0–19.8
Canine	0.50 ± 0.081	75–120	5.31–10.35
Swine	0.726 ± 0.079	100–140	10.94–16.48
Murine	0.043 ± 0.00	500–700	1.59–1.89

Note that in all mouse lungs, the MPA was cannulated with a 0.043 cm radius catheter.

Discussion

Murray's Law, originally proposed to optimize the balance between pumping power and rate of metabolic energy dissipation, predicts that mean flow is proportional to the cube of vessel radius. However, when the assumption of fully developed laminar flow is relaxed to include a range of flow profiles from parabolic to blunt, this exponent varies between 2.3 and 3. Building on previous analyses that considered the role of pulsatile flow in minimizing impedance within branching networks, our analysis demonstrates that in a fully developed pulsatile flow regime, the exponent depends only on the Womersley number, varying between 2.1 and 3. These findings provide a quantitative extension of prior qualitative observations [8,9], while also highlighting discrepancies with previous theoretical work [10].

To validate the applicability of the fully developed steady (traditional) and fully developed pulsatile (modified) Murray's Law to pulmonary arteries, we examined the dependence of the exponent on species and Womersley number. Our results show significant deviations from Murray's Law. Specifically, the mean exponent values found were ∼2.3 in humans, 2.1 in pigs and dogs, and 2.6 in mice, all lower than the canonical exponent of 3.0 predicted by traditional Murray's Law and not entirely well represented by the modified Murray's Law for nonzero-mean pulsatile flow. As shown in Fig. 2, there are some discrepancies between the theoretical predictions and the data across species. Numerical and physiological factors may contribute to these discrepancies. While this study focuses on pulmonary arteries, the influence of the Womersley number on the exponent is likely applicable to other vascular networks, including the aorta and systemic circulation.

For swine, canine, and some human data, the Womersley numbers fall within a moderate range where pulsatile flow dynamics and impedance-based optimization assumptions are most valid. However, at low Womersley number where viscosity dominates, the

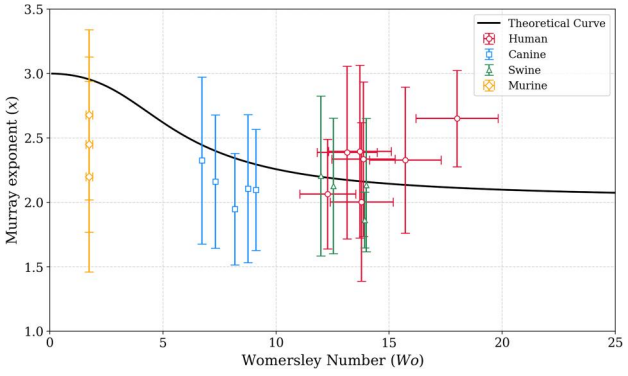

Fig. 2 The theoretical curve for nonzero-mean pulsatile flow (solid line) compared with species-specific data at the MPA (circles, squares, triangles, and diamonds)

impedance function becomes flat, and changes in radius have minimal impact on the cost function. This makes optimization poorly conditioned and highly sensitive to small errors. Additionally, murine vessels have much smaller radii, and the Murray exponents were computed through optimization for each individual bifurcation. In such small vessels, even minor measurement errors can lead to large inaccuracies in the estimated exponent.

Physiologically, two key assumptions in our analysis are symmetric branching and Newtonian rheology. To account for asymmetric branching, the approach developed by Stephenson and Lockerby [7] provides a strong theoretical foundation. However, incorporating an assumption regarding relative flow distribution among branches is necessary to optimize the impedance for asymmetric bifurcations with pulsatile flow. The work of Aroesty and Gross [24] on pulsatile fully developed flow of a Casson (i.e., non-Newtonian) fluid in a single cylindrical tube provides a useful framework for relaxing the Newtonian fluid assumption.

Limitations

Several additional limitations must be acknowledged. First, our study was limited by a small sample size, particularly for the murine group ($n = 3$). Given the natural variability in vascular geometry within a species, a larger sample size would strengthen the findings and allow for more reliable and generalizable conclusions. Second, the resolution of the imaging data limits the ability to capture the smallest vessel branches, leading to an incomplete representation of the arterial network. Since higher resolution imaging was performed for the smallest species used, we were able to consistently quantify vessels' radii and lengths to the sixth generation in each species. Third, noise introduced during the image segmentation process may affect the accuracy of vessel boundary identification. Notably, Bartolo et al. demonstrated the importance of accurately defining vessel radii and lengths when generating high-fidelity subject-specific hemodynamic models [25]. This prior study revealed variation in the raw networks, especially in the smallest vessels, even when segmenting the same images multiple times with the same user and standard segmentation procedures. Fourth, all canine and murine samples in this study were male, while the swine were all female, introducing a potential confounding factor, as sex-based differences are known to influence pulmonary vascular structure and function [26].

Physiological factors not considered in the analysis include non-Newtonian blood viscosity (which varies with vessel diameter), wall compliance (also dependent on vessel diameter), branching angles, asymmetric bifurcations and trifurcations, as well as nonlaminar flow features that contribute to energy dissipation. The influence of these factors across species remains unclear. Therefore, investigating the sources of discrepancies between theoretical predictions and empirical data across species represents an important direction for future research.

Conclusions

In this study, we revisited Murray's Law by analyzing imaging data from four species: humans, canines, swine, and murine. We found that the average Murray exponents in all cases were lower than the predicted value of 3.0 from the classical formulation. We also present an impedance analysis to derive a numerical relationship between the Murray exponent and the Womersley number for nonzero-mean fully developed pulsatile flow. Under these conditions, the optimal exponent varies with Womersley number, ranging from 2.1 to 3.0. Finally, we compared this theoretical curve to species-specific data using values measured at the MPA. Except for the murine data, which did not follow the trend, the theoretical curve captured the overall pattern reasonably well in swine, canine, and some humans at moderate Womersley values. Our findings highlight the need for a more generalized framework to refine predictions of optimal branching structures in physiological networks relevant to pulmonary vascular behavior and adaptation.

Acknowledgment

S.A.C. received funding support from the Balsells Fellowship. M. J.C. was funded by TL1TR001415. N.C.C. was supported through R01HL154624 and R01HL147590. We would also like to acknowledge Professor Megan Miller from the Virginia Military Institute, John Miller from North Carolina State University, Professor Mette Olufsen from North Carolina State University, and Alina Lily Jones from University of California, Irvine for their contributions.

Funding Data

- Balsells Fellowship.
- TL1TR001415.
- R01HL154624 and R01HL147590.

Data Availability Statement

The datasets generated and supporting the findings of this article are obtainable from the corresponding author upon reasonable request.

References

[1] Murray, C. D., 1926, "The Physiological Principle of Minimum Work: I. The Vascular System and the Cost of Blood Volume," Proc. Natl. Acad. Sci., **12**(3), pp. 207–214.
[2] Zamir, M., 1978, "Nonsymmetrical Bifurcations in Arterial Branching," J. Gen. Physiol., **72**(6), pp. 837–845.
[3] Uylings, H. B. M., 1977, "Optimization of Diameters and Bifurcation Angles in Lung and Vascular Tree Structures," Bull. Math. Biol., **39**(5), pp. 509–520.
[4] Olufsen, M. S., Peskin, C. S., Kim, W. Y., Pedersen, E. M., Nadim, A., and Larsen, J., 2000, "Numerical Simulation and Experimental Validation of Blood Flow in Arteries With Structured-Tree Outflow Conditions," Ann. Biomed. Eng., **28**(11), pp. 1281–1299.
[5] Taber, L. A., 1998, "An Optimization Principle for Vascular Radius Including the Effects of Smooth Muscle Tone," Biophys. J., **74**(1), pp. 109–114.
[6] Kassab, G. S., 2006, "Scaling Laws of Vascular Trees: Of Form and Function," Am. J. Physiol.-Heart Circ. Physiol., **290**(2), pp. H894–H903.
[7] Stephenson, D., and Lockerby, D. A., 2016, "A Generalized Optimization Principle for Asymmetric Branching in Fluidic Networks," Proc. R. Soc. A: Math., Phys. Eng. Sci., **472**(2191), p. 20160451.
[8] West, G. B., Brown, J. H., and Enquist, B. J., 1997, "A General Model for the Origin of Allometric Scaling Laws in Biology," Science, **276**(5309), pp. 122–126.
[9] Painter, P. R., Edén, P., and Bengtsson, H.-U., 2006, "Pulsatile Blood Flow, Shear Force, Energy Dissipation and Murray's Law," Theor. Biol. Med. Modell., **3**, p. 31.
[10] Shumal, M., Saghafian, M., Shirani, E., and Nili-Ahmadabadi, M., 2024, "A General Scaling Law of Vascular Tree: Optimal Principle of Bifurcations in Pulsatile Flow," J. Appl. Fluid Mech., **17**(10), pp. 2203–2214.
[11] Sherman, T. F., 1981, "On Connecting Large Vessels to Small. The Meaning of Murray's Law," J. Gen. Physiol., **78**(4), pp. 431–453.
[12] McCulloh, K. A., Sperry, J. S., and Adler, F. R., 2003, "Water Transport in Plants Obeys Murray's Law," Nature, **421**(6926), pp. 939–942.
[13] Zhou, B., Cheng, Q., Chen, Z., Chen, Z., Liang, D., Munro, E. A., Yun, G., et al., 2024, "Universal Murray's Law for Optimised Fluid Transport in Synthetic Structures," Nat. Commun., **15**(1), p. 3652.
[14] Ritman, E. L., and Zamir, M., 2012, *The Physics of Pulsatile Flow*, Springer, New York, NY.
[15] Updegrove, A., Wilson, N. M., Merkow, J., Lan, H., Marsden, A. L., and Shadden, S. C., 2017, "SimVascular: An Open Source Pipeline for Cardiovascular Simulation," Ann. Biomed. Eng., **45**(3), pp. 525–541.
[16] Seiter, D. P., Allen, B., Tabima, D. M., Hacker, T. A., Corrado, P., Oechtering, T. H., Reeder, S. B., Chesler, N. C., and Wieben, O., 2022, "4D Flow MRI Analysis of Flow, Velocity, and Cardiac Flow Compartments in a Swine Model of Pulmonary Hypertension," 31st Annual Meeting ISMRT-ESMRMB, London, UK, May 7–12.
[17] Mulchrone, A., Kellihan, H. B., Forouzan, O., Hacker, T. A., Bates, M. L., Francois, C. J., and Chesler, N. C., 2019, "A Large Animal Model of Right Ventricular Failure Due to Chronic Thromboembolic Pulmonary Hypertension: A Focus on Function," Front. Cardiovasc. Med., **5**, p. 189.
[18] Vanderpool, R. R., Kim, A. R., Molthen, R., and Chesler, N. C., 2011, "Effects of Acute Rho Kinase Inhibition on Chronic Hypoxia-Induced Changes in Proximal and Distal Pulmonary Arterial Structure and Function," J. Appl. Physiol., **110**(1), pp. 188–198.
[19] Fedorov, A., Beichel, R., Kalpathy-Cramer, J., Finet, J., Fillion-Robin, J.-C., Pujol, S., Bauer, C., et al., 2012, "3D Slicer as an Image Computing Platform for the Quantitative Imaging Network," Magn. Reson. Imaging, **30**(9), pp. 1323–1341.
[20] Hernandez-Cerdan, P., 2024, "SGEXT: Spatial Graph Extractor," GitHub, Inc., San Francisco, CA, accessed Aug. 2024, https://github.com/phcerdan/SGEXT
[21] Chambers, M. J., Colebank, M. J., Qureshi, M. U., Clipp, R., and Olufsen, M. S., 2020, "Structural and Hemodynamic Properties of Murine Pulmonary Arterial Networks Under Hypoxia-Induced Pulmonary Hypertension," Proc. Inst. Mech. Eng., Part H: J. Eng. Med., **234**(11), pp. 1312–1329.

[22] Avram, R., Tison, G. H., Aschbacher, K., Kuhar, P., Vittinghoff, E., Butzner, M., Runge, R., et al., 2019, "Real-World Heart Rate Norms in the Health eHeart Study," NPJ Digital Med., **2**(1), p. 58.
[23] Janssen, P. M., Biesiadecki, B. J., Ziolo, M. T., and Davis, J. P., 2016, "The Need for Speed: Mice, Men, and Myocardial Kinetic Reserve," Circ. Res., **119**(3), pp. 418–421.
[24] Aroesty, J., and Gross, J. F., 1972, "The Mathematics of Pulsatile Flow in Small Vessels I. Casson Theory," Microvasc. Res., **4**(1), pp. 1–12.
[25] Bartolo, M. A., Taylor-LaPole, A. M., Gandhi, D., Johnson, A., Li, Y., Slack, E., Stevens, I., et al., 2024, "Computational Framework for the Generation of One-Dimensional Vascular Models Accounting for Uncertainty in Networks Extracted From Medical Images," J. Physiol., **602**(16), pp. 3929–3954.
[26] Martin, Y. N., and Pabelick, C. M., 2014, "Sex Differences in the Pulmonary Circulation: Implications for Pulmonary Hypertension," Am. J. Physiol.-Heart Circ. Physiol., **306**(9), pp. H1253–H1264.